

Evaluating Airborne Remote Sensing ET Estimates using Eddy Covariance Systems and a Heat Flux Source Area Function

José L. Chávez^{1, 2, ‡}, Terry A. Howell^{2, ‡}, Prasanna H. Gowda^{2, ‡},
Christopher M.U. Neale^{2, *}, Paul D. Colaizzi^{2, ‡}

[‡]Conservation and Production Research Laboratory
USDA-Agricultural Research Service
P.O. Drawer 10, Bushland, TX 79012-0010

*Biological and Irrigation Engineering
Utah State University, Logan, UT

Abstract

The use of water for production of crops must become more efficient as competition for water increases. Thus, saving water by managing irrigation systems better may be possible if irrigation scheduling is improved by accurately estimating spatially distributed actual evapotranspiration (ET). ET can be estimated using energy balance algorithms that use agrometeorological and remote sensed surface reflectance/temperature data. In this study, the objective was to evaluate spatial ET estimates obtained with a modified energy balance-based Two Source Model (TSM). For this purpose, two high-resolution aircraft images acquired during the 2008 Bushland Evapotranspiration and Agricultural Remote Sensing Experiment (BEAREX08) at the USDA-ARS Conservation and Production Research Laboratory, Bushland, TX, were used. Predicted ET values for cotton fields were compared with measured ET from eddy covariance systems using a heat flux source area function. Results showed that the TSM slightly under estimated ET by 0.5 mm d⁻¹, (or -5.1%) with a standard deviation of 0.6 mm d⁻¹. Overall, the modified TSM performed well for LAI values less than 1.5 m² m⁻².

Keywords: Southern High Plains, semi-arid environment, remote sensing, two source energy balance model, water management.

¹ Corresponding author, email: jose.chavez@ars.usda.gov

² Agricultural Engineer, Agricultural Engineer and Research Leader, Agricultural Engineer, Agricultural Engineer and Agricultural Engineer respectively.

Introduction

Remote sensing (RS) derived evapotranspiration (ET) values can potentially be used as input for irrigation scheduling and for hydrologic simulations. In addition, seasonal ET may be used to assess the overall irrigation project efficiency, provided volumes of water pumped (or diversions) had been measured.

Most of the RS algorithms used to estimate crop ET are based on the land surface energy balance (EB) model. These algorithms are based on the fact that ET is a change of the water state, from liquid to vapor, depending on available energy (net radiation at the surface less the energy into the ground), Su et al. (2005).

Remote sensing based surface energy balance for land provides instantaneous estimates of latent heat flux (LE) or evapotranspiration (ET). Using remote sensing inputs in the energy balance equation has been recognized as a feasible method to mapping spatially distributed crop water use (Jackson, 1984).

In terms of remote sensing based EB models, there are several algorithms available in the literature. Gowda et al. (2008) present a description and discussion on most of the EB models that use remote sensing inputs for agricultural water management. Most of the EB models are single source models, e.g. SEBI (Menenti and Choudhury, 1993), SEBAL (Bastiaanssen et al., 1998), SEBS (Su, 2002), METRIC (Allen et al., 2007), etc. These models estimate different components of the EB assuming that the surface heat fluxes

originate from a source that is the composite of vegetation and background soil (substrate).

However, there is a fundamental problem in representing a heterogeneous (sparse, non-uniform) surface as a single layer or source because of the significant influence of the soil/substrate on the total surface EB. Thus, the surface resistance to evaporation has lost physical meaning because it represents an unknown combination of stomatal resistance of the vegetation and resistance to soil evaporation (Blyth and Harding, 1995). This resulted in the development of two-source approaches or models (TSM), where the energy exchanges of the soil/substrate and vegetation are evaluated separately (Shuttleworth and Wallace, 1985). The TSM is a more physically based model that differentiates or partitions the EB terms, net radiation (R_n), sensible heat flux (H), and latent heat flux (LE) between the soil and the vegetation canopy, (Norman et al., 1995).

Norman et al. (1995) and Kustas and Norman (1999, 2000) developed operational methodology for the two-source approach proposed by Shuttleworth and Wallace (1985) and Shuttleworth and Guerney (1990). Their model showed good agreement with observations [made with meteorological flux stations, eddy covariance (EC)/Bowen ratio EB systems] over sub-humid prairie, semi-arid shrub, and fully irrigated crops. The TSM methodology generally does not require additional meteorological or information over single-source models; however, it requires some assumptions such as the partitioning of composite radiometric surface temperature into soil and vegetation components, turbulent exchange of

mass and energy at the soil level, and coupling/decoupling of energy exchange between vegetation and substrate (i.e., parallel or series resistance networks). The energy exchange in the soil-plant-atmosphere continuum is based on resistances to heat and momentum transport, and sensible heat fluxes are estimated by the temperature gradient-resistance system. Radiometric temperatures, resistances, sensible heat fluxes, and latent heat fluxes of the canopy and soil components are derived by iterative procedures constrained by composite, directional radiometric surface temperature, vegetation cover fraction, and maximum potential latent heat flux.

In an evaluation study, Chávez et al. (2008) found out that the Norman et al. (1995) and Kustas and Norman (1999) TSM algorithm for low biomass (leaf area index, LAI, less than $3 \text{ m}^2 \text{ m}^{-2}$) resulted in large under predictions of ET. They added that the ensemble sensible heat flux was better estimated when the surface aerodynamic resistance term was eliminated from the sensible heat flux originating from the ground, in the parallel resistance network model.

Regarding the evaluation of ET, estimated from remote sensing imagery and a EB model, using measured ET by eddy covariance (EC) systems, Chávez et al. (2005) demonstrated that using heat flux source area functions (footprint models) was more appropriate than employing simple area of interest (AOI) polygons that average ET pixels upwind of the eddy covariance tower location.

In this study, a modified TSM, Chávez et al. (2008), was applied to very high spatial resolution airborne remote sensing imagery acquired over cotton fields in the Southern High Plains (SHP) to derive ET. Furthermore, spatially

distributed ET pixels were weighted and integrated using a heat source area function (footprint) for comparison to ET measured with eddy covariance systems in order to assess the performance of the modified TSM.

Materials and Methods

Study area

Field data collection and coinciding acquisition of high resolution remote sensing data was made during the 2008 cotton cropping season at the USDA-ARS Conservation and Production Research Laboratory (CPRL), located in Bushland, Texas. The geographic coordinates of the CPRL are 35° 11' N, 102° 06' W, and its elevation is 1,170 m above mean sea level. Soils in and around Bushland are classified as slowly permeable Pullman clay loam. The major crops in the region are corn, sorghum, winter wheat, and cotton. Wind direction is predominantly from the south/southwest direction. Annual average precipitation is about 562 mm while about 670 mm of water are needed to grow cotton. Although, only 280 mm of water (depth) fall as precipitation during the cotton growing season (New, 2005).

Eddy covariance

Eddy covariance is based on the direct turbulent measurements of the product of vertical velocity fluctuations (w') and a scalar (e.g. air temperature, water vapor, carbon dioxide, horizontal wind speed, etc.) concentration fluctuation (c') producing a direct measurement of H, LE, CO₂, and momentum

(shear forces) fluxes respectively, under the assumption that the mean vertical velocity is zero. If turbulence is treated as a set of fluctuations about a mean value, which is called Reynolds averaging, then the value of any variable at a given time is the sum of a temporal mean (over some time period) plus an instantaneous deviation. EC principles and history can be found in Hipps and Kustas (2001), and Shuttleworth (2007) respectively. Burba and Anderson (2007) provide an on-line guidelines for EC method installation, use, maintenance, data post-processing, etc.

Two identical EC systems were installed on the East weighing lysimeter experimental fields managed under irrigation (a NE field and a SE field; Fig. 1), [4.7 ha each, i.e. 210 m wide (East-West) × 225 m long (North-South)], close to the center of the field and downwind of the predominant wind direction. Cotton was planted on May 21, 2008, on these East fields, and these fields started being irrigated (lateral move) on May 23. The NE field had North-South row orientation while the SE field had East-West row orientation. Each EC system consisted of a fast response 3D sonic anemometer (model CSAT3³, Campbell Scientific Inc., Logan, UT), a fast response open path infrared gas (H₂O and CO₂) analyzer (model LI-7500, LI-COR Inc., Lincoln, NE), a fine wire thermocouple (model FW05, Campbell Scientific Inc., Logan, UT), an air temperature/humidity sensor (model HMP45C, Vaisala Inc., Woburn, MA), and a micrologger (model CR3000, Campbell Scientific Inc., Logan, UT). A constant air density measured as the

³ The mention of trade names of commercial products in this article is solely for the purpose of providing specific information and does not imply recommendation or endorsement by the U.S. Department of Agriculture.

mean for each 15-min period was used (model CS106, Vaisala PTB110 barometer, Campbell Scientific, Logan, UT) to compute the flux terms.

The EC system measured turbulent fluxes at a 20-Hz frequency (20 measurements per second) and 15-min average LE and H fluxes were computed. Both EC systems were installed at a 2.5 m height above ground level. The sonic anemometer sensor was oriented towards the predominant wind direction, with an azimuth angle of 225 degree from true North. The magnetic declination angle was taken into account in the EC program.

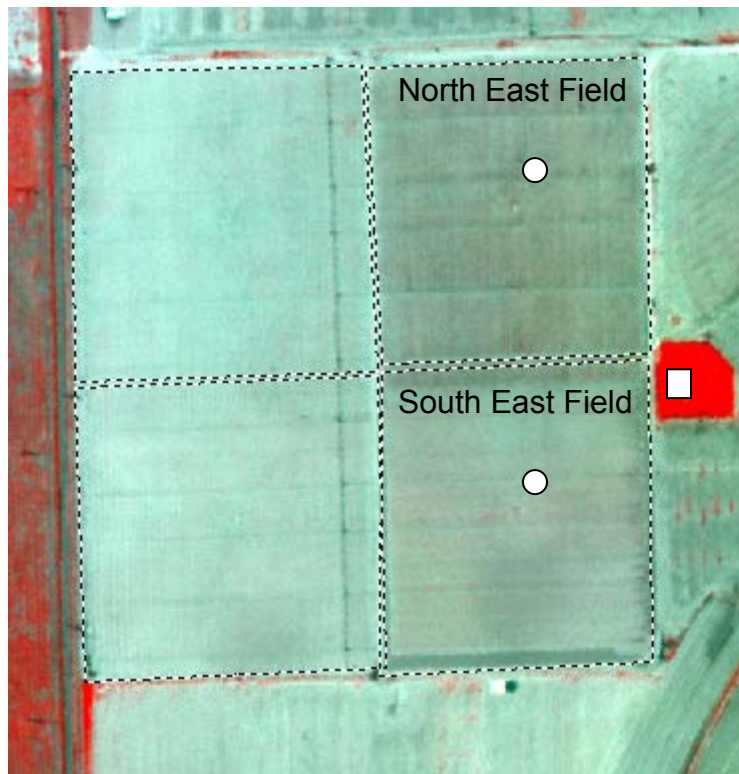


Figure 1. Three-band false color composite reflectance image, DOY 178, showing location of eddy covariance towers (circles) and grass reference weather station (square).

Airborne Remote Sensing Data

The Utah State University (USU) airborne digital multispectral system was used to acquire multispectral remote sensing data at 1-m spatial resolution for visible and near-infrared, and 4-m for thermal-infrared portions of the electromagnetic spectrum. This is a third generation of the system originally described by Neale and Crowther (1994), based on digital frame cameras but following similar image calibration procedures. The USU multispectral system comprises of three Kodak Megaplug digital frame cameras with interference filters centered in the green (Gn) (0.545-0.560 μm), red (0.665-0.680 μm), and near-infrared (0.795-0.809 μm) portions of the electromagnetic spectrum. The fourth camera is an Inframetrics 760 thermal-infrared scanner (8-12 μm) that provides imagery to obtain surface radiometric temperature images.

Two airborne remote sensing images/scenes were used, each acquired over the CPRL on June 26 (DOY 178), and July 28 (DOY 210), respectively. All images were acquired close to 11:30 a.m. CST to coincide with Landsat 5 TM or ASTER satellite overpasses. These images were calibrated and transformed into surface reflectance and temperature images to be used for the estimation of reflected outgoing short wave and long wave radiation, respectively, with both components required in the estimation of spatially distributed net radiation.

Two source energy balance model

To derive LE (or ET_i) Eq. 1 is solved for LE, i.e., as a residual of the surface EB equation (Brown and Rosenberg, 1973, and Stone and Horton, 1974):

$$R_n = G + H + LE \quad (1)$$

where, R_n is net radiation, G is the soil heat flux, and H is sensible heat flux. Units in Eq. 1 are all in $W\ m^{-2}$; with R_n positive toward the crop surface and other terms positive away from the crop surface. The conversion of LE to ET as an hourly and daily rate is detailed in the appendix.

This EB model mainly needs, remotely sensed radiometric surface temperature (T_{sfc} , K), air temperature (T_a , K), horizontal wind speed (U , $m\ s^{-1}$), leaf area index (LAI, $m^2\ m^{-2}$), vegetation fraction cover (f_c), fraction of LAI that is green (f_g), crop height (h_c , m), average leaf width (w , m), and net radiation (R_n) as input. The remote sensing input dependent variables, among others, are T_{sfc} , LAI, h_c , f_c , surface albedo, etc. In addition, the model needs weather data such as air temperature, horizontal wind speed, incoming short wave solar radiation, and relative humidity values; which were taken from the ARS weather station (ARS-Bushland, square symbol in Fig. 1) at Bushland, TX.

The TSM algorithm solves Eq. 1 for LE after finding separately the canopy R_n and H and the soil R_n , G and H components, i.e. the TSM partitions each of the surface energy balance components into fluxes generated from the

vegetation canopy (first source) and the bare soil/background soil (second source) as depicted in Fig. 2. For instance, the ensemble H was estimated by summing sensible heat fluxes from both soil (H_s) and canopy (H_c). H_s occurs between the soil surface and a point above the canopy (Z_h) where air temperature (T_a) is measured, while H_c is generated between the vegetation canopy and a parcel of air at Z_h , assuming a parallel resistance network (Fig. 2).

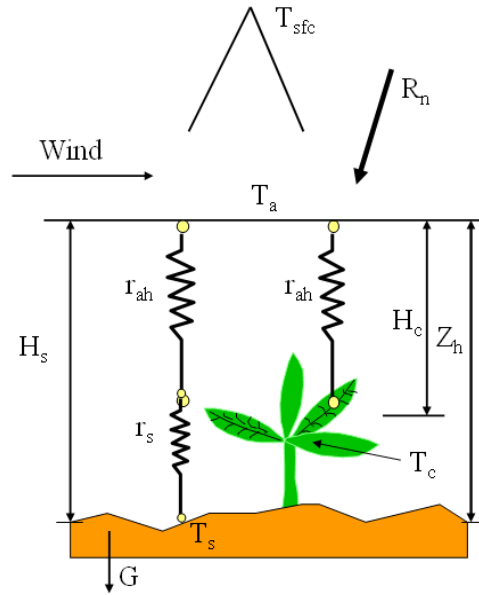


Figure 2. TSM parallel resistance network scheme.

Mathematically H is expressed as:

$$H = H_c + H_s \quad (2)$$

$$H_c = \frac{\rho_a C p_a (T_c - T_a)}{r_{ah}} \quad (3)$$

$$H_s = \frac{\rho_a C p_a (T_s - T_a)}{(r_{ah} + r_s)} \quad (4)$$

$$r_s = \frac{1}{[0.004 + (0.012 U_s)]} \quad (5)$$

where, T_c is canopy temperature (K), T_s is soil temperature (K), r_s is the resistance to heat flow above the soil ($s\ m^{-1}$), r_{ah} is the surface aerodynamic resistance ($s\ m^{-1}$) to heat transfer, U_s is horizontal wind speed ($m\ s^{-1}$) just above the soil surface, ρ_a is air density ($kg\ m^{-3}$), and C_{p_a} is specific heat of dry air ($1,004\ J\ kg^{-1}\ K^{-1}$). T_c and T_s were estimated using Eq. 6 for a Nadir looking thermal infrared remote sensor as:

$$T_{sfc} = \left[(f_c \times T_c^4) + ((1 - f_c) \times T_c^4) \right]^{\frac{1}{4}} \quad (6)$$

where, T_{sfc} is the so-called “ensemble (or composite) radiometric surface temperature,” and f_c is the fractional vegetation cover (function of LAI). First, to obtain H , an initial estimation of H_c , applying the Priestley and Taylor (1972) ET model, is performed. Subsequently, the H_c value is used to derive an initial T_c value by inverting Eq. 3 assuming a neutral atmospheric stability condition. Next, Eq. 6 is solved for T_s and updated values of H_c and H_s are computed correcting r_{ah} for atmospheric stability using the Monin-Obukhov (MO) atmospheric stability length scale (similarity theory, Foken, 2006). The MO mechanism is explained in detail in Chávez et al. (2005). T_c and T_s were verified by testing the estimated LE for a negative value, in which case temperatures are not correct, and then the soil is assumed to have a dry surface. A new iteration cycle is needed, in which LE is set to zero for the soil component and H_s is re-calculated. A new T_s and T_c

values are found and sensible heat flux components are again estimated, and canopy LE computed. In this parallel resistances network, r_{ah} was eliminated from the computation of H_s considering it may yield better H_s (H) estimates for sparser vegetation according to Chávez et al. (2008).

Soil heat flux (G , in $W\ m^{-2}$) was estimated using three different methods because different remote sensing based G models are developed under different conditions, i.e. crop type, soil background, soil/vegetation moisture levels, etc; thus there was the need to find a suitable G model that would yield accurate values for the cotton fields under the conditions encountered at the CPRL. The first model used was that (Eq. 7) developed by Chávez et al. (2005). A second model was from Norman et al. (1995), who estimated G as a function of the net radiation at the soil surface only (Eq. 8).

$$G = \{(0.3324 - 0.024\ LAI) \times (0.8155 - (0.3032\ \ln[LAI]))\} \times R_n \quad (7)$$

where LAI is leaf area index ($m^2\ m^{-2}$). The G model is valid for the range of LAI values between 0.3 and 5.0 $m^2\ m^{-2}$. This G model is a combination of linear-logarithmic functions and was developed using measured data on corn and soybean fields near Ames, Iowa, and airborne remote sensing based LAI and R_n estimates.

$$G = 0.35 \times R_{n_soil} \quad (8)$$

where R_{n_soil} ($W\ m^{-2}$) is the net radiation at the soil surface (soil only) in $W\ m^{-2}$.

Also, the G model developed by Bastiaanssen (2000) was applied (Eq. 9). This model was developed using a wide variety of soil vegetation cover types:

$$G = \left\{ T_B (0.0038 + 0.0074 \alpha) \times (1 - 0.98 \text{NDVI}^4) \right\} \times R_n \quad (9)$$

where T_B (°C) is remotely sensed brightness (at sensor) surface temperature, i.e. the resulting temperature from converting the remote sensing thermal band digital numbers to radiance (system calibration) and then to temperature (Planck's law) without any further atmospheric interference calibration. Normalized difference vegetation index (NDVI) is determine using reflectance values from the red and near-infrared bands. Surface albedo (α) was computed according to Brest and Goward (1987) as a function of surface reflectance in the red and near-infrared bands.

Heat flux source area (footprint) model

In an effort to understand and define the upwind area that contributes with heat fluxes to eddy covariance (or Bowen ratio) system 'flux area source' or footprint models have been developed. The footprint models determine what area upwind of towers is contributing with heat fluxes to the sensors, as well as the relative weight of each particular cell (sub-area) inside the footprint limits. Different footprint models have been proposed, one-dimensional (1D), and two-dimensional (2D) models. These models are the analytical solution to the diffusion-dispersion-advection equation (Horst and Weil, 1992 and 1994). Other models are Lagrangian (Leclerc and Thurtel, 1990). Studies using these models

were able to prove that depending on the height of the vegetation, height of the instrumentation, wind speed, wind direction standard deviation, and atmospheric stability condition the shape and length of the footprint would vary upwind of the instruments, as well as the relative weights (magnitude of contribution), in each individual cell/area inside the footprint. Areas very close to the station contribute less to the total flux sensed by the instrument, areas further away (upwind) increasingly contribute more, up to a point where a peak is reached, thereafter the contribution decreases rapidly further upwind from the station (Verma, 1998). Similar behavior describes the crosswind flux distribution detected by the instruments.

In this study the Flux Source Area Model (FSAM) by Schmid (1994) was used to integrate and weight the TSM estimate ET values. The FSAM was based on the Horst and Weil (1992) model (coded in Fortran) generates the footprint weights for the source area and the approximate dimensions of the footprint area for an area that contributes up to 90% of the sensed fluxes by the instrumentation. It includes the crosswind-integrated flux as Horst and Weil (1992, 1994):

$$F(x,y,Z_m) = D_y(x,y) \cdot \overline{F^y}(x,Z_m) \quad (10)$$

where, $F(x,y,Z_m)$ is the footprint weight function, $D_y(x,y)$ is the cross-wind distribution function, and $\overline{F^y}(x,Z_m)$ is the cross-wind integrated function.

Results and Discussion

During DOY 178, the weather conditions were such, relative humidity (RH) was low and wind speed (U) was high. Thus, the grass reference ET was higher on DOY 178 than DOY 210 (Table 1). In addition, incoming short wave solar radiation (R_s) was slightly higher for DOY 178 than DOY 210. Additional weather and crop parameter values can be found in Table 1 below. Table 1 also shows the cotton height (h_c) and its leaf area index (LAI) during both DOYs. These two DOYs were selected for analysis since wind direction (U dir) was from the south southwest direction, the direction of predominant winds, i.e. sufficient fetch.

Table 1. Weather and crop conditions on DOY 178 and 210.

	DOY	
	178	210
R_s , $W\ m^{-2}$	980	963
T_a , $^{\circ}C$	31.6	30.8
RH, %	31	44
U, $m\ s^{-1}$	7.6	4.9
U dir, $^{\circ}$	206	214
U dir std, $^{\circ}$	20	20
h_c , m	0.18	0.64
LAI, $m^2\ m^{-2}$	0.1	1.3
ET_o , $mm\ d^{-1}$	10	8

In the process of correcting the surface aerodynamic temperature for atmospheric stability, the Monin-Obukhov stability length was computed (L), as shown in Table 2. This parameter was also used in the FSAM footprint to determine the extent of the footprint and the individual cell weight value within the boundary of the footprint. It is worth noting that L was considerably large on DOY 210, which indicates that H was very small. Consequently, the cotton field was using most of the available energy ($R_n - G$) for the evapotranspiration process instead of heating the air. Another terms used in the footprint model was the EC sensors' height (Z_m) and the friction velocity (u_*) (Table 2).

Table 2. Variables and parameters used in the footprint FSAM.

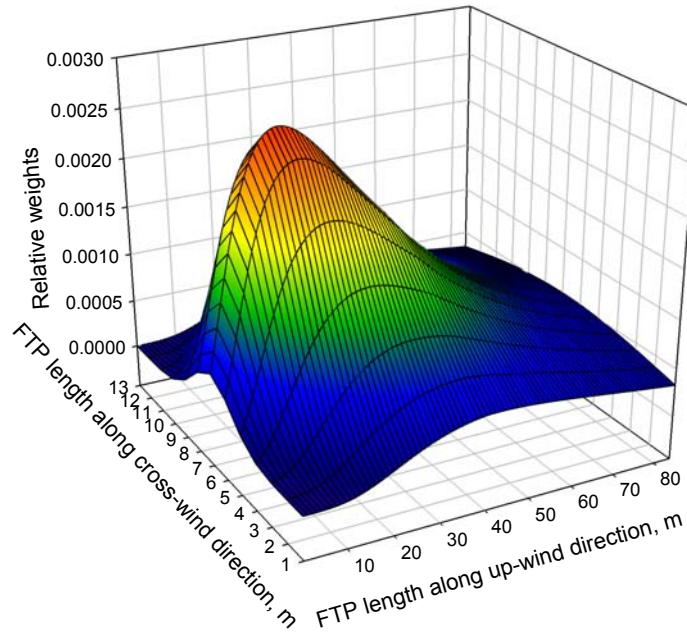
DOY	$u_*, \text{ m s}^{-1}$	$r_{ah}, \text{ s m}^{-1}$	$L, \text{ m}$	$Z_m, \text{ m}$
178	0.48	34.5	-65.2	2.5
210	0.53	25.5	-1071.5	2.5

According to the FSAM, for DOY 178, 90% of the upwind footprint length (fetch) was 84 m and the crosswind length was only 13 m. The leading edge of the footprint started about 6 m (upwind) from the EC tower location. Even though the footprint dimensions were generated for 90% of the fetch, the weights integrated under the footprint function added up to 1, i.e. accounting for 100% of the weights. In the case of DOY 210 weather/crop conditions, the FOOTPRINT fetch was a little bit longer, 105 m, and the crosswind extent was 17 m (not much wind direction variability), with the leading edge stating at 10 m from the EC

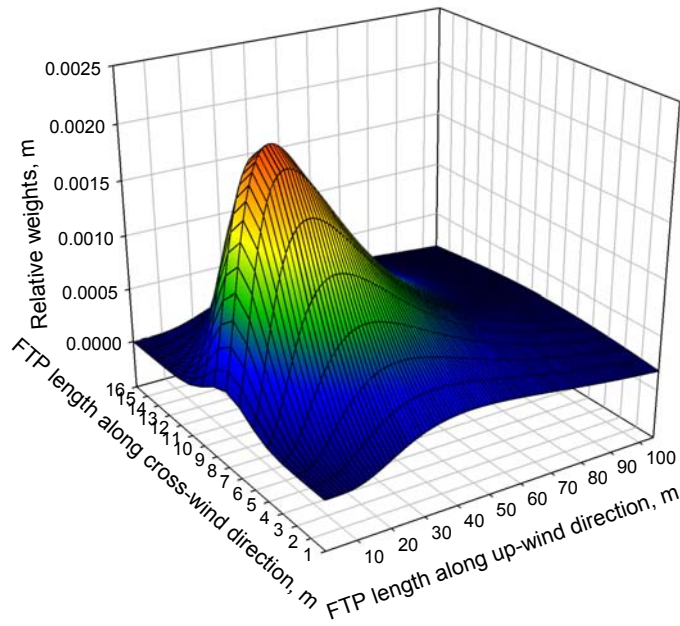
tower. A graphical representation of the footprints, for DOY 178 and 210, can be seen in Figure 3 (a) and (b), respectively. The stronger wind speed of DOY 178 resulted in a rather small footprint extent. Figure 3 also shows the relative weights generated inside the footprint boundary. These weights were used to integrate the remote sensing based TSM ET estimation for comparison to the EC-based ET measurements. The ET weighting and integration procedure followed was that developed by Chávez (2005) and Chávez et al. (2005).

After generating the footprint weights, their text file was converted into an image. Subsequently, the weights image was geo-referenced (rectified) to the same coordinate system/projection/datum (UTM, m) as the reflectance/thermal imagery considering the footprint dimensions and leading edge from the EC tower location as well as the upwind wind direction.

Figure 4 depicts the superposition of the geo-rectified footprint weights image (black and white rectangles) over false color reflectance images of DOYs 178 and 210 respectively (two different days same northeast and southeast fields). The white color in the footprint image represents the concentration of larger (heavy) weights. Multiplying the geo-rectified footprint weights image by the TSM estimated ET image (ET map, Figs. 5 and 6) one obtains the footprint weighted ET values. These values were extracted from the image attribute tables and integrated according to the image pixel value histogram.



(a)



(b)

Figure 3. FSAM 3D footprint representation for DOY 178 (a) and 210 (b).

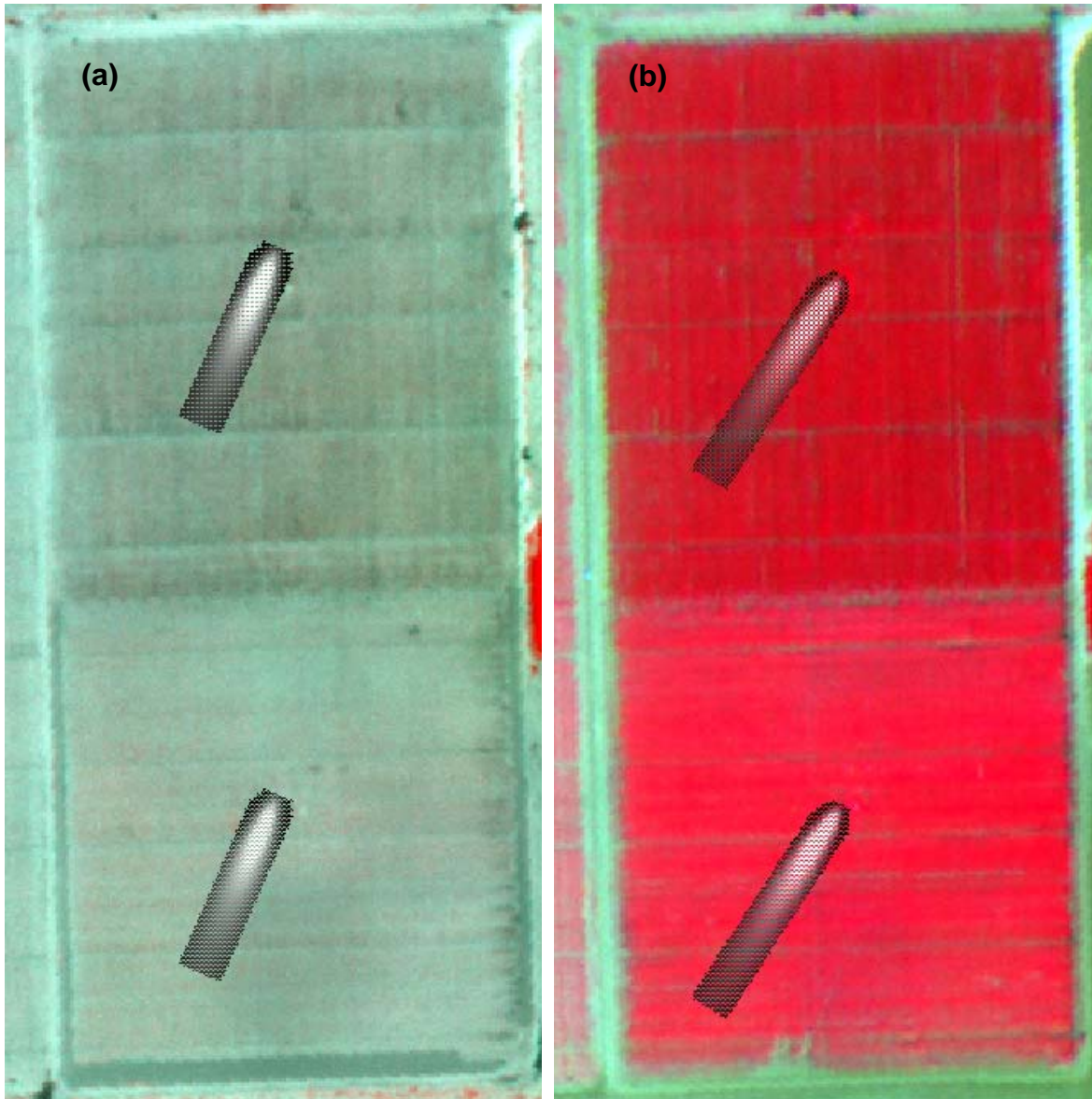


Figure 4. FSAM footprints on DOY 178 (a) and DOY 210 (b) over reflectance images. Both images (a) and (b) are the same northeast fields.

In the process of obtaining ET using the TSM, radiometric surface temperature (T_{sfc}) values were partitioned into canopy (T_c) and background soil temperatures (T_s) using the modification in the calculation of the sensible heat flux originated from the soil. Results from the TSM ensemble surface temperature were reported in Table 3. These temperature values (Table 3) were

used in the estimation of the composite sensible heat flux reported in Table 4. During DOY 178, the soil temperature was about 10°C warmer than the canopy temperature, while on DOY 210 this difference was only 2°C for the NE cotton field and almost 4°C for the SE field. The much lower soil temperatures of DOY 210 were due to the higher biomass and greater ground cover presence (Table 1) on this day, even though solar radiation (R_s , Table 1) was slightly higher on DOY 178.

Table 3. Canopy (T_c) and soil temperature (T_s) from radiometric surface temperature (T_{sfc}).

DOY	Site	T_{sfc} , °C	T_c , °C	T_s , °C
178	NE	42.2	31.6	42.6
178	SE	41.6	31.5	41.9
210	NE	29.2	30.5	32.5
210	SE	30.9	30.6	34.4

As previously discussed above, H was very low during DOY 210 (Table 4), lower for NE cotton field than for the SE field, an indication of higher ET rate at the NE field.

In contrast, H was very high during DOY 178, which indicates that the available energy was used to heat the air and the soil since the cotton plants were very short with not much biomass and probably due to limited soil water content. The resulting H was somewhat over estimated by the modified TSM algorithm. Sensible heat flux estimation error was 15 W m^{-2} (standard deviation, σ_d , of 15.7 W m^{-2}), i.e. an error of $17.2 \pm 15.5\%$. Thus, H result is an indication of good canopy and soil temperature partitioning.

Table 4. Net radiation (R_n), soil (G)/sensible (H) heat flux and ET estimated by the TSM.

DOY/Site	178/NE	178/SE	210/NE	210/SE
R_n , $W\ m^{-2}$	625.9	619.7	719.9	690.4
G, $W\ m^{-2}$	109.3	114.6	73.1	78.1
H, $W\ m^{-2}$	261.8	247.2	17.0	24.0
ET, $mm\ d^{-1}$	4.1	4.2	8.9	8.2

Soil heat flux was better estimated by the Bastiaanssen's model in a comparison with measured G by soil heat flux plates (accounting for heat storage). Bastiaanssen's model predicted G with an average error of only $-9.9\ W\ m^{-2}$ (σ_d of $20.2\ W\ m^{-2}$). In percent based on mean values these were -7.1% average error with a σ_d of 13.6% , while Chávez et al. (2005) model produced G estimates with large errors, in the order of 100% . This result was somewhat expected since the former was developed for a wider range of crops (including cotton), while the latter was developed using measured G values obtained on corn and soybean fields. In the case of the third G model, the errors were 46.6% in average, with a σ_d of 30.1% , thus not suitable for this study. Therefore, Bastiaanssen's G model was used in the TSM applied in this research. Soil heat flux values, using Bastiaanssen's model, can be found in Table 4, for individual fields and DOYs.

Net radiation was estimated accurately by the TSM, the average estimation error was only $39.8\ W\ m^{-2}$ (σ_d of $7.9\ W\ m^{-2}$), or in percent $6.5 \pm 1.6\%$. Table 4 shows the individual net radiation values for each DOY and field location.

ET, according to the footprint integrated TSM estimation, doubled on DOY 210 with respect to the ET rate of DOY 178 (Table 4). In addition, when the TSM ET values of Table 4 were compared to values measured by the EC systems it turned out that the TSM slightly under predicted ET by 0.5 mm d^{-1} (std of 0.6 mm d^{-1}), or by $5.1 \pm 7.2\%$, respectively. This under prediction is relatively small if one considers that the uncertainty associated with the instrumentation, (for each term of the energy balance) in general ranges from 10-20%. In this study, ET was better predicted than in another research where a satellite image was used and no modification was made on the TSM for the calculation of H; in which case, ET resulted in an under-prediction error of 0.8 mm d^{-1} (std of 0.8 mm d^{-1}), or by $9.2 \pm 9.0\%$ respectively, Chávez et al. (2007). It is important to have in mind that in the latter case no footprint model was used and the pixel resolution was coarser.

This result was evidence that the modification proposed in Chávez et al. (2008) for the TSM to estimate H for the ground, under sparse/low biomass levels, is appropriate. Furthermore, the FSAM footprint seems to be a viable means to weight/integrate very high spatial resolution ET map pixels.

Finally, maps of distributed ET are shown in Figures 5 and 6 for DOY 178 and 210 respectively. As per the distributed ET values in both Fig. 5 and 6, the NE cotton field showed more ET heterogeneity (variability) for DOY 178 than for DOY 210. Also, Figure 5 shows the SE field bordering with a much drier fallow winter wheat field. This situation could have been an issue had the wind speed been calm because the heat flux source area would have extended into the drier

fallow land. Thus, the result would have been a lower ET measurement, by the eddy covariance system, since the drier fallow land had a very low ET rate.

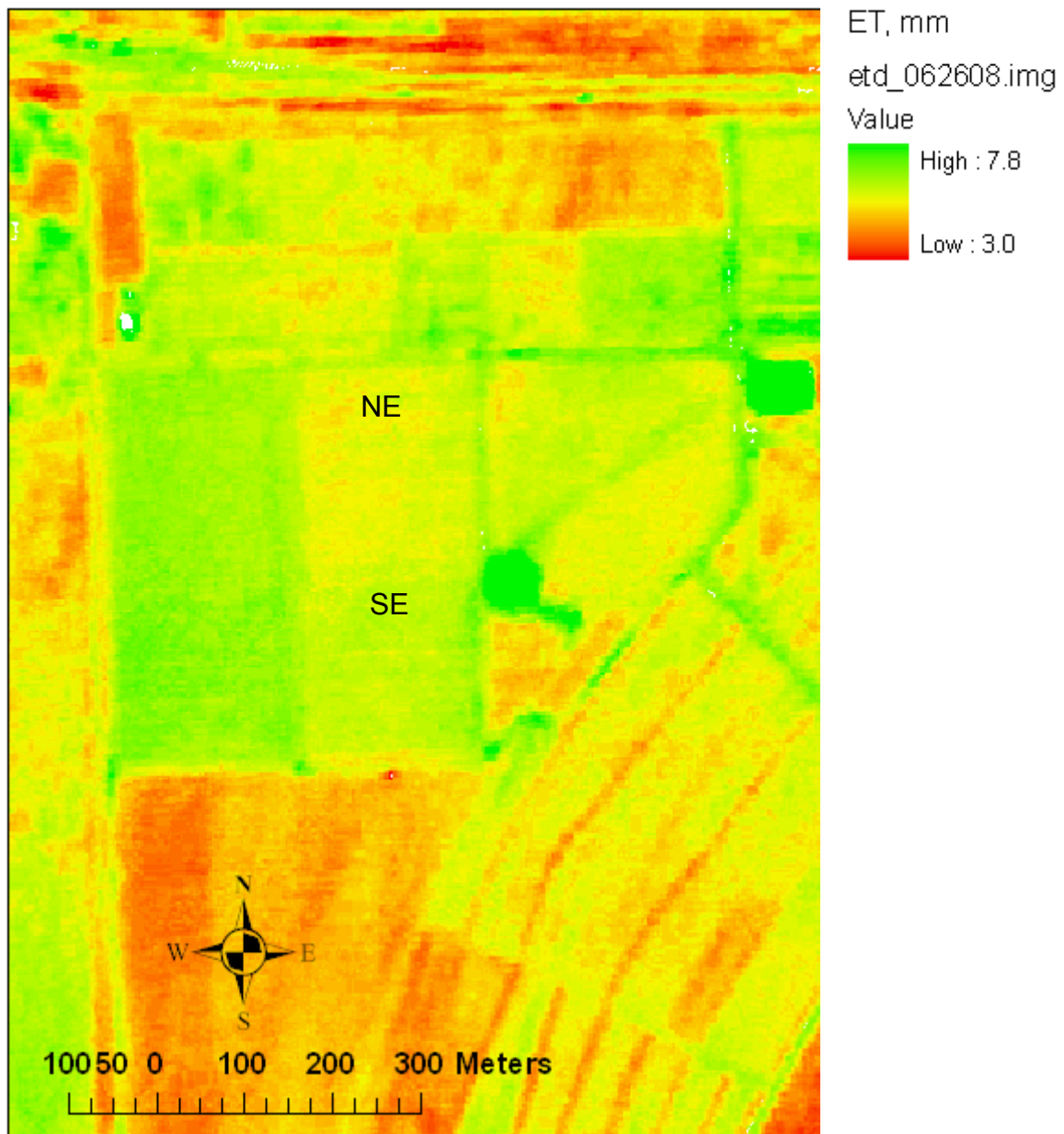


Figure 5. Map of distributed evapotranspiration (ET) generated with the TSM for DOY 178

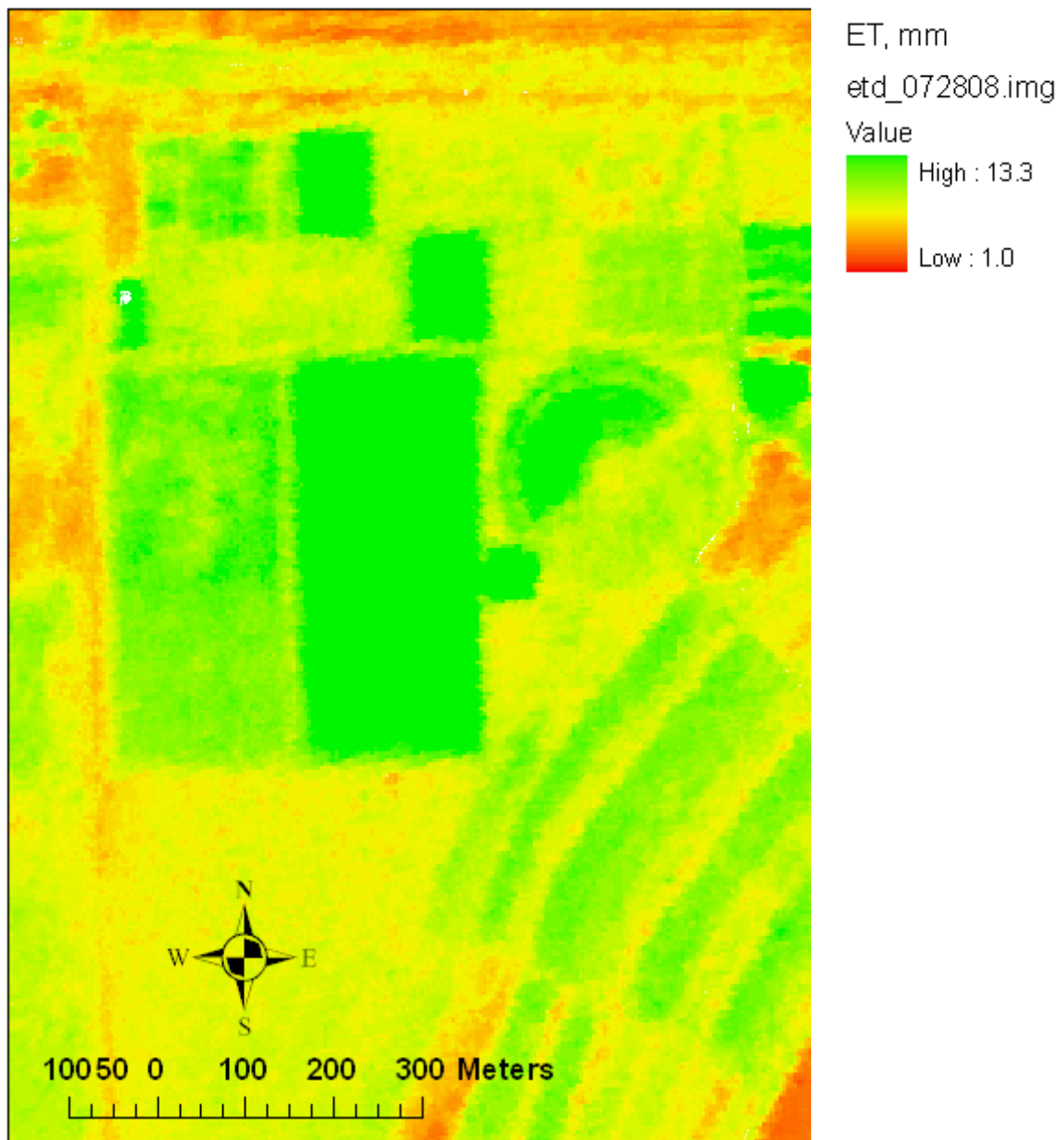


Figure 6. Map of distributed evapotranspiration (ET) generated with the TSM for DOY 210

CONCLUSION

A modified two source energy balance model was applied to very high resolution airborne multispectral imagery to generate distributed ET values. Resulting spatial ET values were weighted and integrated using a 2D heat flux footprint model.

Results indicated that the modification proposed by Chávez et al. (2008) for the TSM sensible heat flux estimation originating from the ground (substrate), under sparse/low biomass levels, was appropriate. Furthermore, the FSAM footprint seems to be a viable means to weight/integrate very high spatial resolution ET map pixels.

In addition, soil heat flux needs to be estimated by a remote sensing-based model valid, i.e. which has been calibrated, for the vegetation/soil background conditions encountered during the scene (image) acquisition. In other words, a soil heat flux model is needed which has been developed for the type of crops, crop biomass level (range of LAI values), soil type(s) and water content levels normally encountered in the study region covered by the remote sensing system.

Further research should include the incorporation of a number of airborne scenes (several different days during the mid-to-end crop growing season) to test the modified TSM under dense biomass presence. This verification would be warranted because the surface resistance network modification suggests ignoring the sensible heat flux originated from the substrate for leaf area index values larger than $3 \text{ m}^2 \text{ m}^{-2}$; which was not covered in this study.

REFERENCES

- Allen, R.G., M. Tasumi, and R. Trezza. 2007. Satellite-based energy balance for mapping evapotranspiration with internalized calibration (METRIC)-model. *ASCE J. of Irrig. and Drain. Eng.* 133(4): 380-394.
- ASCE-EWRI. 2005. The ASCE standardized reference evapotranspiration equation. Report by the American Society of Civil Engineers (ASCE) Task Committee on Standardization of Reference Evapotranspiration. Allen, R.G., I.A. Walter, R.L. Elliot, T.A. Howell, D. Itenfisu, M.E. Jensen, and R.L. Snyder (eds.), ASCE, 0-7844-0805-X, 204 pp., Reston, VA.
- Bastiaanssen, W.G.M., M. Menenti, R.A. Feddes, and A.A. Holtslang. 1998. A remote sensing surface energy balance algorithm for land (SEBAL): 1. Formulation. *J. of Hydrol.* 212-213:198-212.
- Bastiaanssen, W.G.M. 2000. SEBAL-based sensible and latent heat fluxes in the irrigated Gediz Basin, Turkey. *J. of Hydrol.* 229: 87-100.
- Blyth, E.M., and R.J. Harding. 1995. Application of aggregation models to surface heat flux from the Sahelian tiger bush. *Agric. For. Meteorol.* 72: 213-235.
- Brest, C.L., and S.N. Goward. 1987. Driving surface albedo measurements from narrow band satellite data. *International J. of Remote Sensing*, 8:351-367.
- Brown, K.W., and N.J. Rosenberg. 1973. A resistance model to predict evapotranspiration and its application to a sugar beet field. *Agron. J.* 65(3): 341-347.
- Burba G.G., and Anderson D.J. 2007. Introduction to the eddy covariance method: General guidelines and conventional workflow. LI-COR Biosciences, <http://www.licor.com>, 141 pp. (accessed 10 April 2008).
- Chávez, J.L. 2005. Validating surface energy balance fluxes derived from airborne remote sensing. Ph.D. Dissertation. Biological and Irrigation Engineering Department. Utah State University, Logan, Utah. 277 pp.
- Chávez, J.L., C.M.U. Neale, L.E. Hipps, J.H. Prueger, and W.P. Kustas. 2005. Comparing aircraft-based remotely sensed energy balance fluxes with eddy covariance tower data using heat flux source area functions. *J. of Hydromet.* 6(6):923-940.

- Chávez J.L., Gowda P.H., Howell T.A., Copeland K.S. 2007. Evaluating three evapotranspiration mapping algorithms with lysimetric data in the semi-arid Texas High Plains. *In proceedings of the 28th annual international irrigation show*, Dec. 9-11, 2007, San Diego, CA, Irrigation Assoc. CD-ROM, 268-283.
- Chávez, J.L., P.H. Gowda, T.A. Howell, C.M.U. Neale, and K.S. Copeland. 2008. Estimating hourly crop ET using a two source energy balance model and multispectral airborne imagery. *Submitted to Irrig. Sci. J.*
- Foken, T. 2006. 50 Years of the Monin-Obukhov similarity theory. *Boundary-Layer Meteorol.* 119(3): 431-447.
- Gowda, P.H., J.L. Chavez, P.D. Colaizzi, S.R. Evett, T.A. Howell, and J.A. Tolk. 2008. ET mapping for agricultural water management: Present status and challenges. *Irrig. Sci. J.* 26(3):223-237, DOI 10.1007/s00271-007-0088-6.
- Hipps, L., and W. Kustas. 2001. Patterns and organisation in evaporation. In: Grayson, R. and G. Blöschl (eds.). Chapter 5 in *Spatial patterns in catchment hydrology: observations and modeling*, Cambridge Univ. Press, pp. 105-122, ISBN: 0-521-63316-8.
- Horst, T.W., J.C. Weil. 1994. How far is far enough? The Fetch requirement for micrometeorological measurement of surface fluxes. *J Atmos Ocean Tech* 11: 1018-1025.
- Horst, T.W., J.C. Weil. 1992. Footprint estimation for scalar flux measurements in the atmospheric surface layer. *Boundary-Layer Meteorol.* 59: 279-296.
- Kustas, W.P., and J.M. Norman. 2000. A two-source energy balance approach using directional radiometric temperature observations for sparse canopy covered surfaces. *Agron. J.* 92:847-854.
- Kustas, W.P., and J.M. Norman. 1999. Evaluation of soil and vegetation heat flux predictions using a simple two-source model with radiometric temperatures for partial canopy cover. *Agric. and Forest Meteorol.*, 94: 13-29.
- Menenti, M., and B.J. Choudhury. 1993. Parameterization of land surface evapotranspiration using a location dependent potential evapotranspiration and surface temperature range. In *Proc. Exchange Processes at the Land Surface for a Range of Space and Time Scales*. 561-568, Bolle HJ et al. (eds), IAHS Publ. 212.

- Neale, C.M.U. and B.G. Crowther. 1994. An airborne multispectral video/radiometer remote sensing system: development and calibration. *Remote Sens. of Environ.* 49(3): 187-194.
- New, L.L. 2005. Agri-Partner irrigation result demonstrations 2005. Texas Cooperative Extension Service, Texas A&M University. Available on line at: <http://amarillo.tamu.edu/programs/agripartners/irrigation2005.htm>
- Norman, J.M., W.P. Kustas, and K.S. Humes. 1995. A two-source approach for estimating soil and vegetation energy fluxes form observations of directional radiometric surface temperature. *Ag. and Forest Meteorol.* 77:263-293.
- Priestley, C.H.B., and R.J. Taylor. 1972. On the assessment of surface heat flux and evaporation using large-scale parameters. *Mon. Weather Rev.* 100: 81-92.
- Schmid, H.P. 1994. Source Areas for Scalars and Scalar Fluxes. *Boundary Layer Meteorol.* 67: 293-318.
- Shuttleworth, W.J. and R.J. Gurney. 1990. The theoretical relationship between foliage temperature and canopy resistance in sparse crops. *Quarterly J. of Royal Meteorol. Soc.*, 116: 497–519.
- Shuttleworth, W.J., and J.S. Wallace. 1985. Evaporation from sparse crops – an energy combination theory. *Quartely J. Royal Meteorol. Soc.*, 111: 839-855.
- Shuttleworth, W.J. 2007. Putting the “vap” into evaporation. *Hydrol Earth Syst Sci* 11(1): 210-244.
- Stone, L.R., and M.L. Horton. 1974. Estimating evapotranspiration using canopy temperatures: Field evaluation. *Agron. J.* 66: 450-454.
- Su, H. M.F. McCabe, E.F. Wood, Z. Su, and J.H. Prueger. 2005. Modeling evapotranspiration during SMACEX: Comparing two approaches local- and regional- scale prediction. *J. of Hydromet.*, 6(6): 910-922.
- Su, Z. 2002. The surface energy balance system (SEBS) for estimation of turbulent heat fluxes. *Hydrol. and Earth Syst. Sci.* 6:85-99.
- Verma, S.B. 1998. Flux footprint estimates affected by measurement height, surface roughness and thermal stability. <http://snrsl.unl.edu/georgeb/footprint/fp-title.html>. Access 10 Jun 2004.

APPENDIX

LE Conversion into ET Rates

Once the TSM has produced estimates of latent heat fluxes (LE, W m⁻²), these need to be converted into an equivalent water depth or instantaneous ET rates (ET_i, mm h⁻¹).

LE is converted into ET as follows:

$$ET_i = \frac{(3,600 \text{ } LE)}{(\lambda_{LE} \rho_w)} \quad (11)$$

where, ET_i is hourly ET (mm h⁻¹) calculated from the TSM estimated instantaneous LE (W m⁻²). λ_{LE} is the latent heat of vaporization (MJ kg⁻¹), equal to (2.501 – 0.00236 T_a), being T_a in ° C units, and ρ_w is water density (~ 1 Mg m⁻³). The 3,600 number is a factor to time conversion of s h⁻¹.

In addition, daily evapotranspiration (ET_d) was computed as:

$$ET_d = \left(\frac{ET_i}{ET_{o,i}} \right) \times ET_o \quad (12)$$

where, ET_{oi} is hourly grass reference ET (mm h⁻¹), calculated using the ARS-Bushland weather station hourly data and the ASCE-EWRI (2005) standardized Penman-Monteith method. ET_o is the daily ET (mm d⁻¹) computed by adding up the hourly ET over the course of the entire day, and ET_i is the TSM estimated actual crop instantaneous ET (mm h⁻¹) values.